PROCEEDINGS OF SCIENCE

Hard multi-particle processes at NLO QCD

Andreas van Hameren*
The H. Niewodniczański Institute of Nuclear Physics
Polisch Academy of Sciences
Radzikowskiego 152, 31-342 Krakow, Poland
E-mail: hameren@ifj.edu.pl

The HELAC-NLO Monte Carlo framework for the calculation of hard scattering cross sections at NLO QCD is introduced, and results for the process $p\bar{p} \to t\bar{t} \to W^+W^- b\bar{b} \to e^+\nu_e\,\mu^-\bar{\nu}_\mu\,b\bar{b}$ are presented.

10th International Symposium on Radiative Corrections (Applications of Quantum Field Theory to Phenomenology) - RADCOR 2011
September 26-30 2011
Mamallapuram, India

*Speaker.

PoS(RADCOR2011)006

1. Introduction

With the start of collisions at LHC at 7 TeV, elementary particle physics entered further into the terascale. The immense energy allows for many multi-particle channels to open. Final states with four or more jets together with isolated leptons may be produced thanks to the available phase space, and identified thanks to the large acceptance of the ATLAS and CMS detectors. Such multi-particle processes are intensively studied, because they form backgrounds for, or modify, signals of physics beyond the Standard Model. Correct interpretation of signals of new physics demands the reduction of theoretical uncertainties related to multi-particle processes. In particular large QCD backgrounds need to be under control, and at least to next-to-leading order (NLO) in fixed-order perturbation theory.

2. Helac-NLO

There has been a remarkable progress in recent years to reach next-to-leading (NLO) precision in QCD for processes with four or more final-state particles and/or partons [1,2]. These calculations are considerably more complex than leading-order (LO) calculations, and several difficulties had to be overcome. From this list of calculations, the ones in [2] have been performed with the help of a collection of computer programs recently published under the name HELAC-NLO as a complete tool for such calculations [3].

One of the issues is related to the cancellation of IR divergences, which is ensured to happen formally, but must eventually be implemented for numerical calculations. In HELAC-NLO the implementation HELAC-DIPOLES [4] of the dipole-subtraction method [5] is used for this purpose. It is based on the LO platform HELAC-PHEGAS [6] making use of the universality of the dipole-subtraction method with respect to details of the partonic process. The phase space integration is optimized with the help of KALEU [7].

HELAC is also used to evaluate tree-level amplitudes, whereas the one-loop amplitudes are evaluated with HELAC-1LOOP [8]. It is an explicit implementation of the OPP approach to one-loop calculations [9], using the universal OPP reduction tool CUTTOOLS [10]. Within the OPP approach the non-universal part of a one-loop calculation can be identified as the numerator of the one-loop amplitude over denominator factors containing the loop integration momentum. HELAC-1LOOP computes these by translating them systematically into tree-level objects. The one-loop master integrals are evaluated with ONELOOP [11]. The part of the rational contribution not provided by CUTTOOLS is also included [12].

3. Results for the process $pp(p\bar{p}) \to t\bar{t} \to W^+W^-b\bar{b} \to e^+\nu_e\mu^-\bar{\nu}_\mu b\bar{b}$

Several processes have been calculated at NLO QCD with HELAC-NLO recently. Here we briefly report on the calculation of $pp(p\bar{p}) \to t\bar{t} \to W^+W^-b\bar{b} \to e^+\nu_e\mu^-\bar{\nu}_\mu b\bar{b}$ with complete off-shell effects. Double-, single- and non-resonant top contributions of the order $\mathcal{O}(\alpha_s^3\alpha^4)$ are consistently taken into account, which requires the introduction of a complex-mass scheme for unstable top quarks [13]. Moreover, the intermediate W bosons are treated off-shell. A few examples of one-loop Feynman graphs for the $gg \to e^+\nu_e\mu^-\bar{\nu}_\mu b\bar{b}$ subprocess are presented in Figure 1.

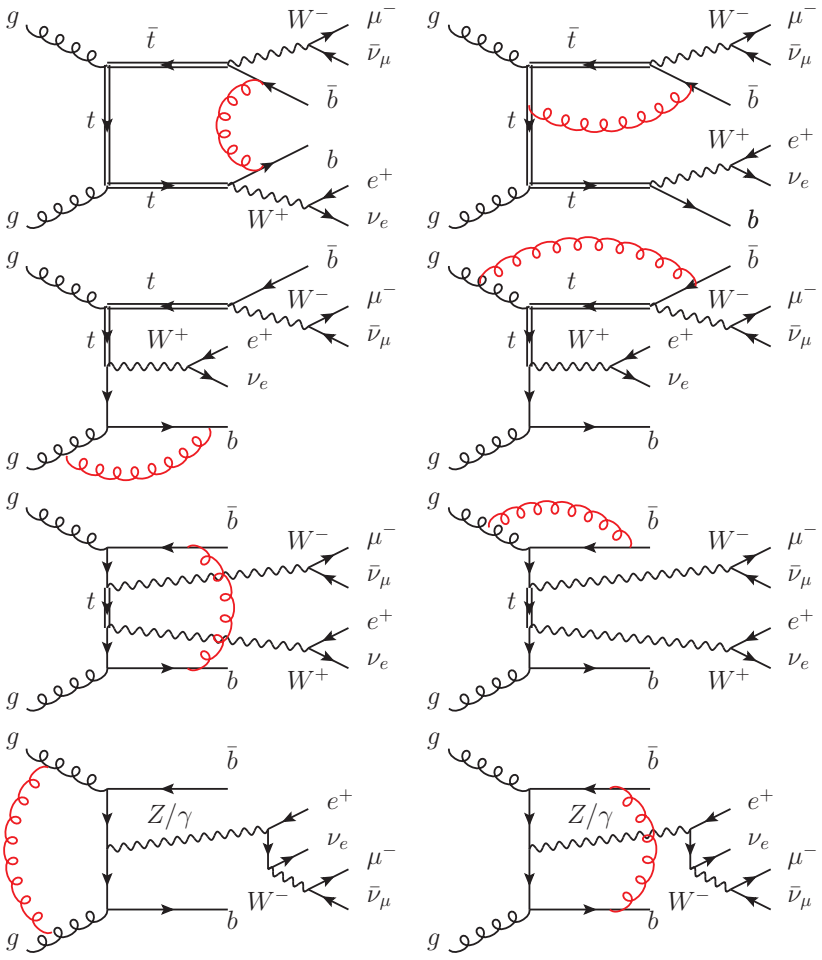

Figure 1: Some one-loop Feynman graphs for the $gg \to e^+\nu_e\mu^-\bar{\nu}_\mu b\bar{b}$ subprocess.

Both center-of-mass energies corresponding to the TeVatron run II and the LHC, *i.e.* $\sqrt{s} = 1.96$ TeV and $\sqrt{s} = 7$ TeV, are considered. The Standard Model parameters are as follows:

$$m_W = 80.398 \text{ GeV}, \quad \Gamma_W = 2.141 \text{ GeV} \tag{3.1}$$

$$m_Z = 91.1876 \text{ GeV}, \quad \Gamma_Z = 2.4952 \text{ GeV} \tag{3.2}$$

$$G_\mu = 1.16639 \times 10^{-5} \text{ GeV}^{-2} \tag{3.3}$$

The electromagnetic coupling and $\sin^2\theta_W$ are derived from the Fermi constant and the masses of the W and Z bosons. The top quark mass is $m_t = 172.6$ GeV and all other QCD partons and leptons are treated as massless. The top quark widths at LO and NLO are $\Gamma_t^{LO} = 1.48$ GeV and $\Gamma_t^{NLO} = 1.35$ GeV where $\alpha_s = \alpha_s(m_t) = 0.10764$. Mass renormalization is performed within the on-shell scheme. All final-state partons with pseudorapidity $|\eta| < 5$ are recombined into jets via the k_T algorithm [14], the *anti-*k_T algorithm [15], or the inclusive Cambridge/Aachen algorithm (C/A) [16] with a cone size of $R = 0.4$. Additional cuts are imposed on the transverse momenta

Algorithm	$\sigma_{\rm LO}$ [fb]	$\sigma_{\rm NLO}$ [fb]
anti-k_T	34.922 ± 0.014	35.697 ± 0.049
k_T	34.922 ± 0.014	35.723 ± 0.049
C/A	34.922 ± 0.014	35.746 ± 0.050

Table 1: *Integrated cross section at LO and NLO for $p\bar{p} \to e^+\nu_e\mu^-\bar{\nu}_\mu b\bar{b} + X$ at the TeVatron run II.*

and the rapidity of two recombined b-jets, namely

$$p_{T_b} > 20 \text{ GeV}, \qquad |y_b| < 4.5. \tag{3.4}$$

To the decay products of the top quarks basic selection cuts are applied:

$$p_{T_\ell} > 20 \text{ GeV}, \;\; |\eta_\ell| < 2.5, \;\; \Delta R_{b\ell} > 0.4, \;\; p_{T_{miss}} > 30 \text{ GeV}. \tag{3.5}$$

The CTEQ6 set of parton distribution functions (PDFs) is consistently used [17]. In particular, CTEQ6L1 with a 1-loop running α_s is used at LO and, CTEQ6M with a 2-loop running α_s at NLO. The contribution from b quarks in the initial state is neglected. The number of active flavors is $N_F = 5$, and the respective QCD parameters are $\Lambda_5^{LO} = 165$ MeV and $\Lambda_5^{MS} = 226$ MeV. In the renormalization of the strong coupling constant, the top-quark loop in the gluon self-energy is subtracted at zero momentum. In this scheme the running of α_s is generated by the contributions of the light-quark and gluon loops. The renormalization and factorization scales, μ_R and μ_F, are set to the common value $\mu = m_t$.

3.1 TeVatron Run II

First we present results for the TeVatron run II. Although the TeVatron has been recently closed, the data analysis in the CDF and D0 experiments is still going on. Therefore, in Table 1 results for the total cross section for the central value of the scale and for the three different jet algorithms mentioned before are presented. The total cross section receives small NLO QCD correction of the order of 2%. Residual scale uncertainties, obtained by varying the scale down and up by a factor of 2, are at the 40% level in the LO case. The dependence is large, illustrating the well known fact that the LO prediction can only provide a rough estimate. As expected, we observe a reduction of the scale dependence going from LO to NLO. In the NLO case we find a variation of the order of 8%. In addition, the size of the non-factorizable corrections, obtained by comparing the full result with the result in the narrow width approximation (NWA), amounts to 1%. This is consistent with the uncertainty of the NWA, which is of the order $\mathcal{O}(\Gamma_t/m_t)$.

In Figure 2, differential cross sections as function of the averaged transverse momentum and the averaged rapidity of the charged leptons are given. Also shown are distributions of missing transverse momentum, $p_{T_{miss}}$, and the dilepton separation $\Delta R_{\ell\ell}$ in the azimuthal angle-pseudorapidity plane. Even though the NLO corrections to the transverse momentum distribution are moderate, they do not simply rescale the LO shape, for they cause distortions at the level of 40%. For $p_{T_{miss}}$, distortions only up to 15% can be observed. As for angular distributions, positive and rather modest corrections of the order of $5\% - 10\%$ are obtained.

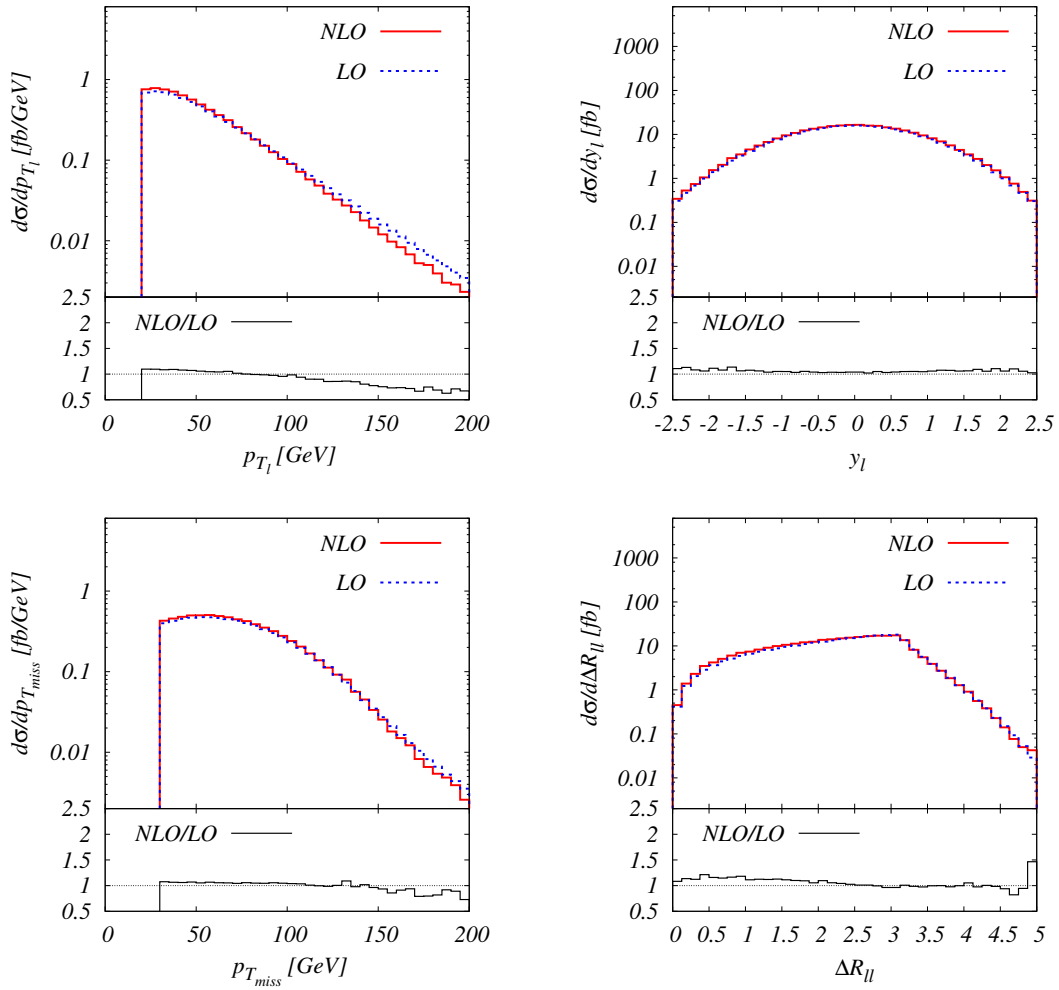

Figure 2: *Differential cross sections for $p\bar{p} \to e^+\nu_e\mu^-\bar{\nu}_\mu b\bar{b} + X$ at the TeVatron run II as a function of the averaged transverse momentum p_{T_ℓ} of the charged leptons, the averaged rapidity y_ℓ of the charged leptons, $p_{T_{miss}}$, and $\Delta R_{\ell\ell}$. The blue dashed curve corresponds to the leading order, whereas the red solid one to the next-to-leading order result. The lower panels display the differential K factor.*

Algorithm	$\sigma_{\rm LO}$ [fb]	$\sigma_{\rm NLO}$ [fb]
anti-k_T	550.54 ± 0.18	808.29 ± 1.04
k_T	550.54 ± 0.18	808.86 ± 1.03
C/A	550.54 ± 0.18	808.28 ± 1.03

Table 2: *Integrated cross section at LO and NLO for $pp \to e^+\nu_e\mu^-\bar{\nu}_\mu b\bar{b} + X$ at the LHC.*

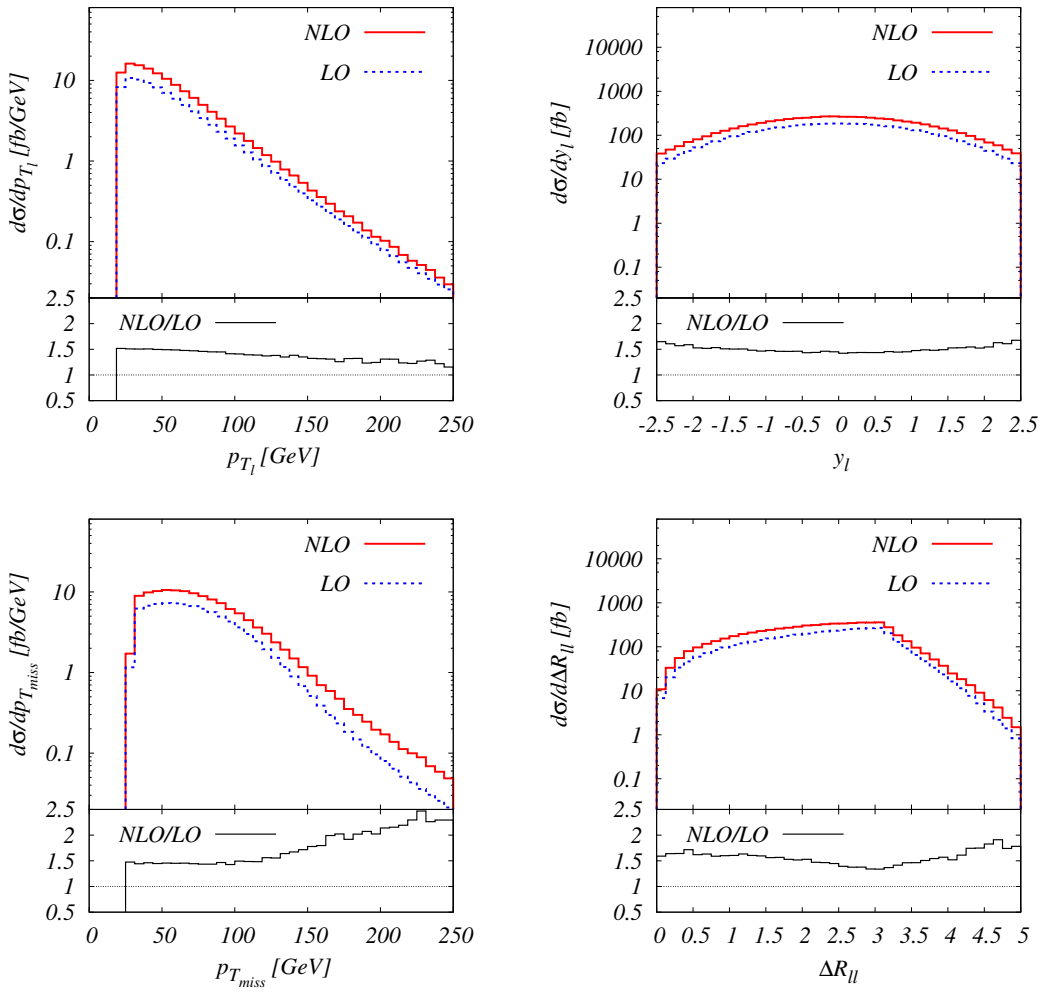

Figure 3: *Differential cross sections for $pp \to e^+\nu_e\mu^-\bar{\nu}_\mu b\bar{b} + X$ at the LHC as function of the averaged transverse momentum p_{T_ℓ} of the charged leptons, the averaged rapidity y_ℓ of the charged leptons, $p_{T_{miss}}$, and $\Delta R_{\ell\ell}$. The blue dashed curve corresponds to the leading order, whereas the red solid one to the next-to-leading order result. The lower panels display the differential K factor.*

3.2 Large Hadron Collider

Table 2 shows the integrated cross sections at the LHC with $\sqrt{s} = 7$ TeV, again for the three different jet algorithms. At the central scale value of $\mu = m_t$, the full cross section receives NLO QCD corrections of the order of 47%. After including the NLO corrections, the large scale dependence of about 37% in the LO cross section is reduced considerably, down to 9%. In order to quantify the size of the non-factorizable corrections for the LHC, a comparison with the narrow-width limit has again been performed. Going from NWA to the full result changes the cross section no more than 1.2% for our inclusive setup.

In Figure 3, differential cross sections as function of the averaged transverse momentum and the averaged rapidity of the charged leptons, along with $p_{T_{miss}}$ and the separation $\Delta R_{\ell\ell}$ are shown.

For the given scale value the NLO QCD corrections are always positive and relatively large. In particular for the p_{T_ℓ} distribution, distortions up to 25% are reached, while for $p_{T_{miss}}$ distortions up to 80% are visible. For the y_ℓ distribution, rather constant corrections up to 50% are obtained. And finally, the distribution of $\Delta R_{\ell\ell}$ acquires corrections even up to 90%.

4. Summary

The Monte Carlo framework HELAC-NLO for the automatic calculation of hard scattering cross sections at NLO QCD was introduced, and results for the process $pp(p\bar{p}) \to t\bar{t} \to W^+W^-b\bar{b} \to e^+\nu_e\mu^-\bar{\nu}_\mu b\bar{b} + X$ obtained with the help of this program were presented. All off-shell effects of top quarks and W bosons were included. The total cross section and an estimate of its scale dependence, along with a few differential distributions were presented, both for the TeVatron run II and the LHC. The impact of the NLO QCD corrections on integrated cross sections at the TeVatron were found to be small, of the order of 2%. At LHC, on the other hand, corrections up to 47% were found. Theoretical uncertainties due to higher order corrections have been estimated to be at the level of 9%. Finally, it has been observed that the corrections affect the overall normalization as well as the shape of differential distributions.

References

[1] A. Bredenstein, A. Denner, S. Dittmaier, S. Pozzorini, JHEP **0808** (2008) 108.
R. K. Ellis, K. Melnikov, G. Zanderighi, JHEP **0904** (2009) 077.
C. F. Berger, Z. Bern, L. J. Dixon, F. Febres Cordero, D. Forde, T. Gleisberg, H. Ita, D. A. Kosower and D. Maitre, Phys. Rev. Lett. **102** (2009) 222001.
A. Bredenstein, A. Denner, S. Dittmaier, S. Pozzorini, Phys. Rev. Lett. **103** (2009) 012002.
R. Keith Ellis, K. Melnikov, G. Zanderighi, Phys. Rev. D **80** (2009) 094002.
C. F. Berger, Z. Bern, L. J. Dixon, F. Febres Cordero, D. Forde, T. Gleisberg, H. Ita, D. A. Kosower and D. Maitre, Phys. Rev. D **80** (2009) 074036.
K. Melnikov, G. Zanderighi, Phys. Rev. D **81** (2010) 074025.
T. Binoth, N. Greiner, A. Guffanti, J. Reuter, J. P. Guillet, T. Reiter, Phys. Lett. B **685** (2010) 293.
A. Bredenstein, A. Denner, S. Dittmaier, S. Pozzorini, JHEP **1003** (2010) 021.
C. F. Berger, Z. Bern, L. J. Dixon, F. Febres Cordero, D. Forde, T. Gleisberg, H. Ita, D. A. Kosower and D. Maitre, Phys. Rev. D **82** (2010) 074002.
T. Melia, K. Melnikov, R. Rontsch, G. Zanderighi, JHEP **1012**, 053 (2010).
C. F. Berger, Z. Bern, L. J. Dixon, F. Febres Cordero, D. Forde, T. Gleisberg, H. Ita, D. A. Kosower and D. Maitre, Phys. Rev. Lett. **106**, 092001 (2011).
A. Denner, S. Dittmaier, S. Kallweit, S. Pozzorini, Phys. Rev. Lett. **106**, 052001 (2011).
T. Melia, K. Melnikov, R. Rontsch, G. Zanderighi, Phys. Rev. **D83**, 114043 (2011).
H. Ita, Z. Bern, L. J. Dixon, F. F. Cordero, D. A. Kosower and D. Maitre, [arXiv:1108.2229 [hep-ph]].

[2] G. Bevilacqua, M. Czakon, C. G. Papadopoulos, R. Pittau, M. Worek, JHEP **0909** (2009) 109.
G. Bevilacqua, M. Czakon, C. G. Papadopoulos, M. Worek, Phys. Rev. Lett. **104** (2010) 162002.
G. Bevilacqua, M. Czakon, A. van Hameren, C. G. Papadopoulos, M. Worek, JHEP **1102** (2011) 083.
G. Bevilacqua, M. Czakon, C. G. Papadopoulos, M. Worek, Phys. Rev. D **84** (2011) 114017.

[3] G. Bevilacqua, M. Czakon, M. V. Garzelli, A. van Hameren, A. Kardos, C. G. Papadopoulos, R. Pittau, M. Worek, [arXiv:1110.1499 [hep-ph]].

[4] M. Czakon, C. G. Papadopoulos, M. Worek, JHEP **0908** (2009) 085.

[5] S. Catani, M. H. Seymour, Nucl. Phys. **B485** (1997) 291-419.
S. Catani, S. Dittmaier, M. H. Seymour, Z. Trocsanyi, Nucl. Phys. **B627** (2002) 189-265.

[6] A. Kanaki, C. G. Papadopoulos, Comput. Phys. Commun. **132** (2000) 306-315.
C. G. Papadopoulos, Comput. Phys. Commun. **137** (2001) 247-254.
A. Cafarella, C. G. Papadopoulos, M. Worek, Comput. Phys. Commun. **180** (2009) 1941-1955.

[7] A. van Hameren, [arXiv:1003.4953 [hep-ph]].

[8] A. van Hameren, C. G. Papadopoulos, R. Pittau, JHEP **0909** (2009) 106.

[9] G. Ossola, C. G. Papadopoulos, R. Pittau, Nucl. Phys. **B763** (2007) 147-169.
G. Ossola, C. G. Papadopoulos, R. Pittau, JHEP **0707** (2007) 085.
G. Ossola, C. G. Papadopoulos, R. Pittau, JHEP **0805** (2008) 004.

[10] G. Ossola, C. G. Papadopoulos, R. Pittau, JHEP **0803** (2008) 042.

[11] A. van Hameren, Comput. Phys. Commun. **182** (2011) 2427-2438.

[12] P. Draggiotis, M. V. Garzelli, C. G. Papadopoulos, R. Pittau, JHEP **0904** (2009) 072.
M. V. Garzelli, I. Malamos, R. Pittau, JHEP **1001** (2010) 040.
M. V. Garzelli, I. Malamos, R. Pittau, JHEP **1101** (2011) 029.
M. V. Garzelli, I. Malamos, Eur. Phys. J. **C71** (2011) 1605.

[13] A. Denner, S. Dittmaier, M. Roth and D. Wackeroth, Nucl. Phys. B **560** (1999) 33.
A. Denner, S. Dittmaier, M. Roth and L. H. Wieders, Nucl. Phys. B **724** (2005) 247 [Erratum-ibid. B **854** (2012) 504].

[14] S. Catani, Y. L. Dokshitzer and B. R. Webber, Phys. Lett. **B285** (1992) 291.
S. Catani, Y. L. Dokshitzer, M. H. Seymour and B. R. Webber, Nucl. Phys. **B406** (1993) 187.
S. D. Ellis and D. E. Soper, Phys. Rev. **D48** (1993) 3160.

[15] M. Cacciari, G. P. Salam and G. Soyez, JHEP **0804** (2008) 063.

[16] Y. L. Dokshitzer, G. D. Leder, S. Moretti and B. R. Webber, JHEP **9708** (1997) 001.

[17] J. Pumplin, D.R. Stump, J. Huston, H.L. Lai, P. Nadolsky, W.K. Tung, JHEP **0207** (2002) 012.
D, Stump, J, Huston, J, Pumplin, W.K. Tung, H.L. Lai, S. Kuhlmann, J.F. Owens, JHEP **0310** (2003) 046.